PERGAMON

Journal of Structural Geology 22 (2000) 865–879

JOURNAL OF STRUCTURAL GEOLOGY

www.elsevier.nl/locate/jstrugeo

A model of normal fault interaction based on observations and theory ☆

Anupma Gupta, Christopher H. Scholz

Lamont-Doherty Earth Observatory and Department of Earth and Environmental Sciences, Columbia University, 61 Route 9W, Palisades, NY 10964, USA

Received 6 April 1999; accepted 26 January 2000

Abstract

Recent earthquakes have shown that fault interaction can affect rupture sequences. However, few criteria are currently available to determine which fault segments are strongly interacting. Here we develop a simple, elastic-plastic model of fault interaction that can assess degrees of interaction within a population of faults using only map traces or displacement profiles. In this model, faults interact through their stress fields. Examination of map traces and displacement profiles from 65 pairs of small ($L < 1$ m) interacting faults shows that faults respond to reductions in shear stress around other nearby faults by accumulating anomalous displacement. There is a positive linear relationship between the amount of stress reduction felt at a tip and anomalous displacement accumulation near this tip. In addition, there is a stress reduction region around faults into which other faults do not propagate and nucleate. The linear relationship and limit to propagation may be used to estimate degrees of interaction within a population of faults. We check for model consistency with observations of separation and overlap, displacement–length ratios, and rift-basin scale fault growth.

1. Introduction

Many recent earthquake sequences, including Landers and Northridge in California and Umbria–Marche in Italy, have involved slip on several interacting fault segments (Sieh et al., 1993; Jones et al., 1994; Amato et al., 1998). These events show that fault interaction can profoundly affect rupture sequences. For example, seismic events may 'jump' across interacting faults and create a larger earthquake than anticipated, such as in the case of Landers (Wesnousky, 1986; Sieh et al., 1993). An important consideration for seismic hazard evaluation is whether an event may jump between segments. The potential for a 'jumping' event partly depends on the degree of static fault interaction between faults. The degree of interaction also affects spatial fault distributions (e.g. Cowie, 1998) and fault population scaling, specifically displacement–length (D–L) and size–frequency distributions (Cartwright et al., 1995; Wojtal, 1996; Cladouhos and Marrett, 1996). These relationships are important constraints on physical models of fault growth. Understanding and quantifying fault interaction are also important to the exploration, geomorphology, and stratigraphy of fault-related structures. In this study we develop a new method and theory to quantify the degree of fault interaction between pairs of faults.

The growth of isolated faults provides a basis for quantification of fault interaction. Theoretical models and observations of natural faults have led to an understanding of the mechanisms and characteristics of isolated fault growth. Isolated faults have constant D–L ratios (Fig. 1) within a particular setting (Dawers et al., 1993; Schlische et al., 1996). The physical basis for the constant D–L ratio is derived in the Dugdale fault growth model (Cowie and Scholz, 1992a). There are two central features of the Dugdale model. First, the stress concentration at the fault tip is finite; when

☆ An electronic annex to this paper is available at http://veo.elsevier.nl/sg/publish/897.

E-mail address: gupta@ldeo.columbia.edu (A. Gupta).

0191-8141/00/$ - see front matter
PII: S0191-8141(00)00011-0

the stress concentration equals the yield strength the fault will propagate (Fig. 1). Second, the maximum displacement–length ratio (D_{max}/L_{max}) depends on the ratio of yield strength to shear modulus of the rock.

Peacock and Sanderson (1991, 1994) were the first to observe that displacement profiles are affected by fault interaction. They found that D–L profiles of interacting faults are asymmetric with steep D–L gradients near interacting tips. The point of maximum displacement in a displacement–length profile, d_{max}, is shifted toward the interacting tip. Elastic boundary element modeling results confirmed that d_{max} is closer to interacting tips and that the average displacement gradient is steeper in the interacting region (Willemse et al., 1996; Willemse, 1997). While the observations of displacement profiles generally agree with boundary element models of fault interaction, presently no quantitative criteria exist to evaluate degrees of fault interaction based on variations in displacement profiles.

Separation–overlap ratios (Fig. 1) provide a crude measure of fault interaction. Aydin and Schultz (1990) measured separation–overlap ratios but did not relate these ratios to their model. Their model shows that underlapping fault tips are favored to propagate towards each other, while overlapping tips are retarded. Huggins et al. (1996) also measured separation–overlap ratios. They acknowledged that separation–overlap ratios provide little information about the interaction state of the overlap zone. Cartwright and Mansfield (1998) measured displacement gradients and suggested that the wide range of gradients in normal faults occur because of fault interaction. Later we show that increasing displacement gradients and anomalous displacement accumulation occur with increasing fault interaction. Thus rather than separation–overlap ratios, displacement anomalies can be used as a proxy for interaction, but, as we shall see, the two are related.

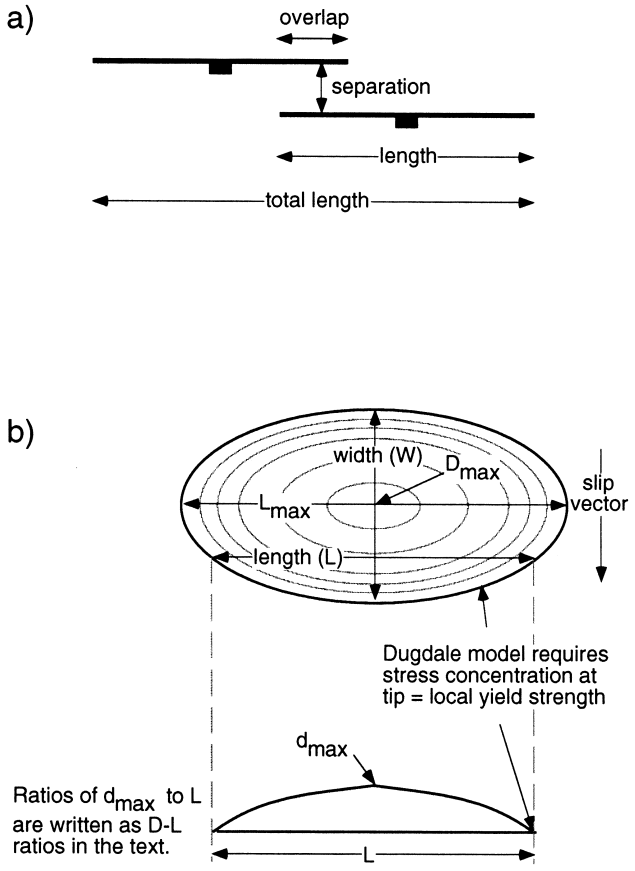

Fig. 1. Terminology used throughout the paper illustrated with (a) map view of interacting fault pair, and (b) elliptical fault plane with displacement (D) contours and displacement–length (D–L) profile shown below. Ratios of d_{max}–L are written as D–L ratios in the remainder of the paper. The condition for stress concentration at crack tips is described by Cowie and Scholz (1992a).

To quantify displacement anomalies near interacting fault tips, we compare D–L profiles of the 'isolated' faults in a population with the remaining interacting population. Using the Dugdale model (Cowie and Scholz, 1992a), and knowledge of stress field variations around isolated elastic cracks (Segall and Pollard, 1980; Willemse et al., 1996), we develop a simple static criterion for fault propagation which takes into account shear stress contributions from nearby faults. Using predictions from this model, we can quantify the degree of interaction between pairs of normal faults using information about their map view configuration and displacement profiles.

2. What is fault interaction and how should we measure it?

Two main types of fault interaction occur. Hard linkage is the case where fault segments are physically linked to another fracture or fault. This interaction changes the geometry of the fault plane (e.g. figure 8 in Gupta and Scholz, 1998). When faults interact only through their stress fields they are soft linked. In this case the geometry of the fault plane does not change significantly. For the faults we study no physical linkage is observed and we assume fault segments are soft linked and interacting only through their stress fields. However, segments may be physically linked outside the plane of observation.

We measured the influence of stress field interaction on displacement by selecting a representative set of 'non-interacting' faults and comparing them to the remaining interacting population. Ideally, to isolate the effects of interaction, well-resolved D–L profiles are required for interacting and non-interacting faults within a homogeneous tectonic setting and rock type. Our fault interaction model is based on a population

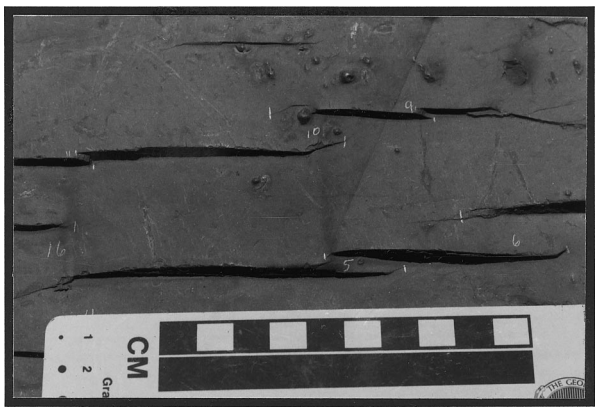

Fig. 2. (a) Map view of normal faults. The picture was taken parallel to a bedding surface that is cut by numerous normal faults. The rock tends to part preferentially along bedding surfaces or along fault planes. The fault scarps appear as shadows.

of faults from the Solite Quarry near Eden, North Carolina, because they closely approximate this ideal data set.

Hundreds of small ($L < 1$ m) normal faults in Mesozoic siltstones are exposed in the Solite Quarry. The deep-water lacustrine siltstones of the Cow Branch Member were deposited within the long, linear Mesozoic Dan River rift basin (Schlische, 1993; Schlische et al., 1996). The Solite Quarry faults all dip toward the basin bounding fault. They lie at high angles to finely laminated bedding of siltstones, which tend to part along bedding planes. With such exposures, accurate measurements can be made of D–L profiles of a large number of faults (Schlische et al., 1996) (Fig. 2).

The size of the faults ($L < 1$ m) permitted measurements to be made in the laboratory, where we illuminated slabs of faulted siltstone so that the fault scarps appeared dark compared to the surrounding rock (Fig. 3a). The image was captured with a digital video camera and then processed to increase contrast using NIH Image software (Fig. 3b). By using a special feature of NIH Image (version 1.43) we could calibrate

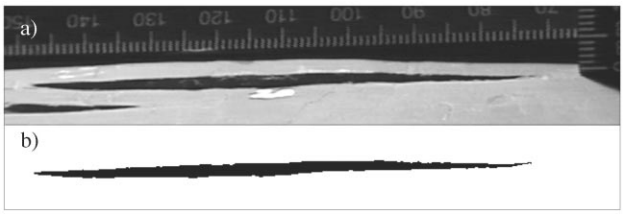

Fig. 3. Fault D–L profile measurement technique. (a) Faults were lit so that scarps appear as shadows. Each fault was photographed with a digital video camera with a millimeter scale along the length and dip of the fault plane. (b) The image was processed to increase contrast and the remaining black and white image was cleaned up. Image analysis software counted the asymmetric black pixels, and we converted the number of pixels to distance in each direction to obtain D–L profiles for each fault studied.

the horizontal and vertical pixel scales independently. Millimeter scales were placed parallel to and along the dip of faults to provide fiducials for the pixel calibration (Fig. 3a). We also scaled the pixel size with fault size by zooming in or out, so that small and large faults were measured with about the same amount of detail. Using this technique, only the portion of the fault with discernible displacement was recognized, even if the fault trace appeared longer in map view.

We sampled only one offset marker layer for each fault, such as in Fig. 2. Often we did not know whether this layer crossed the fault near the center or edge of an elliptical fault plane. The location of the marker layer can affect the observed D–L profile (Muraoka and Kamata, 1983), depending on the shape of the overall displacement distribution. For an elliptical slip distribution, such as in an elastic crack profile (Willemse et al., 1996), D–L ratio does not vary with the observation location (Fig. 4). However, for a cone-shaped distribution (Fig. 4a), D–L ratio varies linearly with distance from the center of the fault plane (Fig. 4c). Most real faults have slip distributions somewhere between the elliptical and conical end members (Rippon, 1985; Barnett et al., 1987; Childs et al., 1995; Gupta and Scholz, 1998). The population of faults from Solite have nearly elliptical D–L profiles (Fig. 4b), meaning that only near the edges of fault planes does the D–L ratio vary significantly from the ratio at the center (Fig. 4c). We minimized this source of variability in the sample of D–L profiles by eliminating any faults that have D–L ratios much lower than the majority of the population.

We selected a subset of the population that is 'non-interacting' to compare with the remaining interacting population. The non-interacting faults are separated from other faults by at least 15% of their total length (Fig. 1a). This criterion is consistent with An's (1997) observation that strike-slip faults do not link if separation is more than 10% of the total length. In addition, a 15% separation value is consistent with boundary element models of normal fault interaction (figure 10 in Willemse, 1997). Willemse finds that as separation becomes greater than 12.5% of length for short faults ($L/W = 2$), the ability of nearby cracks to influence propagation tendency becomes small, even for large overlaps. For the non-interacting set, we also chose faults that have relatively symmetrical D–L profiles; this is because a highly asymmetrical profile is a clear indication of interaction (Peacock and Sanderson, 1991, 1994; Dawers and Anders, 1995; Willemse et al., 1996). Using these selection criteria we obtained 16 characteristic or 'isolated' profiles. Because the non-interacting faults may be affected slightly by fault interaction, the effects of interaction on D–L profiles may be underestimated.

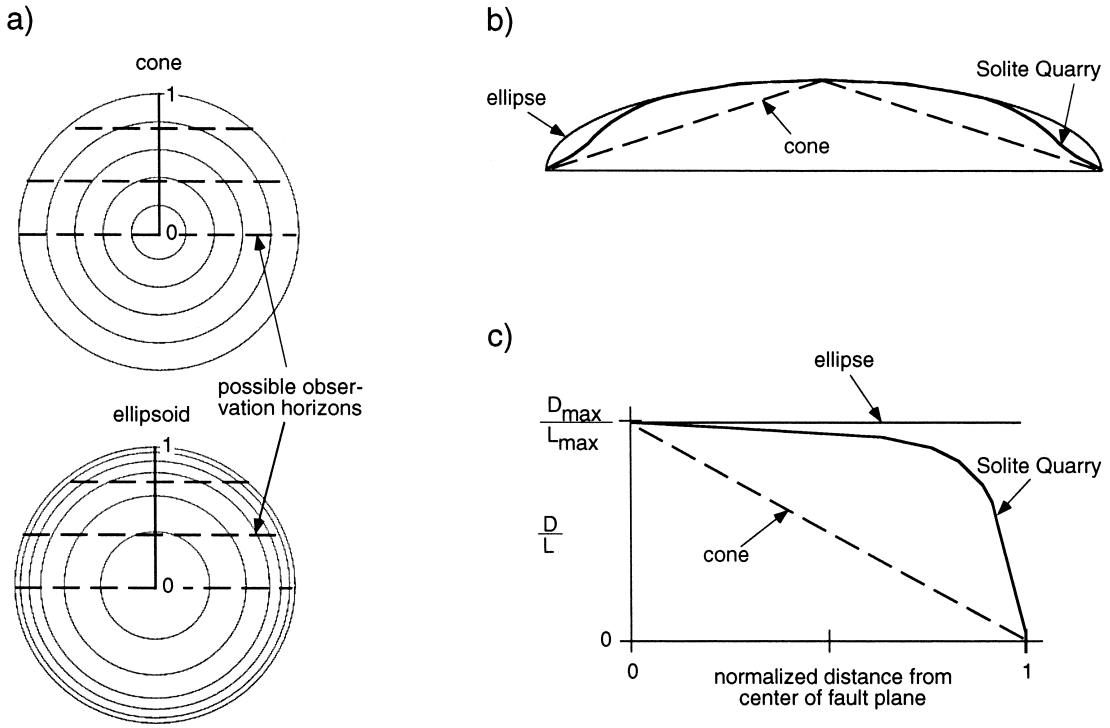

Fig. 4. (a) Circular fault planes with contours of displacement, either cone or half-ellipsoid shaped. Dashed lines indicate possible observation locations. Dark solid line indicates normalized distance from the center of the fault plane. (b) D–L profile for different slip distributions. The Solite Quarry fault population profile is almost the same as that for an elliptical slip distribution except near the tips. (c) D–L ratio vs. normalized distance from the center of the fault plane. For an elliptical distribution, the ratio does not change with sampling location. For a cone-shaped distribution, the ratio decreases linearly with sampling distance from the center of the fault plane. The D–L ratio for the Solite Quarry faults does not change significantly until sampling reaches the edge of the fault plane.

3. Characteristic non-interacting profiles

Our best estimate of an isolated fault profile from the Solite Quarry was found by averaging characteristic profiles (Fig. 5). We cut each displacement–length profile in half along its length and averaged 32 halves instead of 16 complete faults. This approach is justified in that each fault tip is isolated and can grow separately. This enabled us to obtain a better estimate of the variance around the mean profile. We thus obtained a less noisy characteristic profile, without altering the overall shape of the profile. The variance in characteristic displacement profiles partly represents variations in material properties, shape of the fault plane, and location of the observation horizon with respect to the fault plane. Although we could not completely eliminate the influence of these factors, the average or characteristic profile is our best estimate of an isolated fault profile.

The shape of the isolated fault profile may change with material properties, boundary conditions, and growth mechanisms (Cowie and Scholz, 1992a; Bürgmann et al., 1994; Cowie, 1998). Consequently, for each new population studied we must define a new characteristic profile. Comparing faults within a particular population is reasonable if material properties, growth mechanisms, and boundary conditions do not change significantly within the population. One advantage of using characteristic profiles is that we do not need to know the details of how faults accumulate displacement because we assume isolated faults grow by the same processes as interacting faults. The method should work the same for populations of faults that grow by creep, are seismogenic, or that have finite, linear, or zero displacement gradients near the tips.

4. A simple fault interaction model

Though displacement fields in the Solite Quarry faults are obviously permanent now (Fig. 2), we assumed that displacement fields were elastic at the time that these faults stopped growing. We previously validated this assumption by comparing observed fault displacement fields from the Solite Quarry population with an elastic boundary element solution (Gupta and Scholz, 1998). We found that a dislocation model within an elastic material can describe the displacement field around a fault accurately despite the large strains and time scales often associated with faulting.

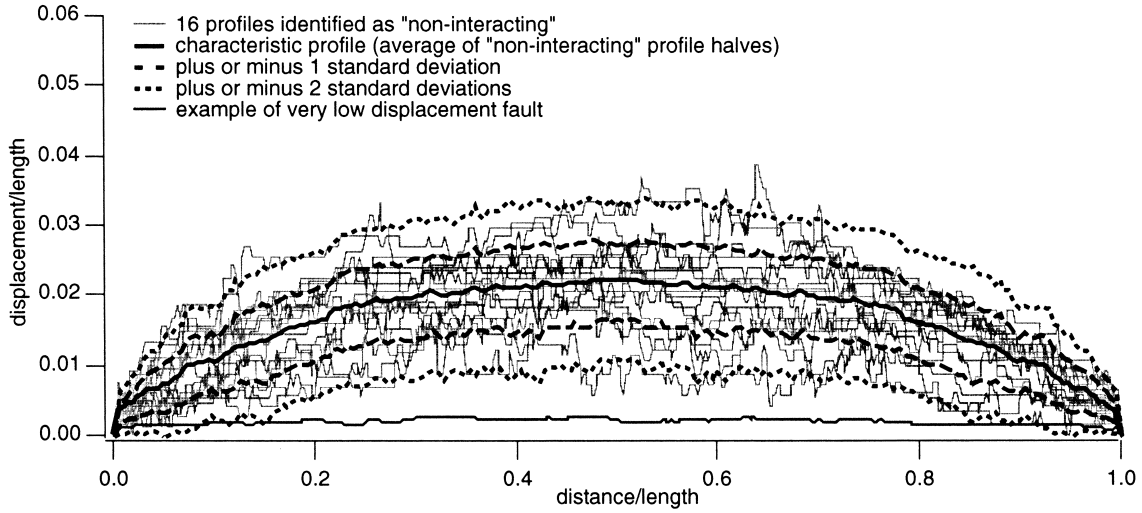

Fig. 5. Characteristic profile. We attempted to obtain the ideal isolated fault profile by selecting as many 'isolated' faults as possible. We found 16 relatively isolated faults (thin gray lines) and averaged all halves (thick solid line). Standard deviations around the mean profile are also shown (thick dashed lines). For comparison, we show a fault with a very low D–L ratio (thin shaded line) that we did not include in our analysis because we may have observed it near the fault tip. In all further analysis, D–L profiles are compared to the characteristic profile (thick solid line) in units of standard deviation.

Because a model with elastic rheology can reproduce observed fault displacement fields, we could assume that the elastic stresses did not relax during fault growth. All accumulated displacement contributed to the stress field around these normal faults. Thus we can define a net static stress drop which is calculated based on the net displacement on these faults. This is analogous to the static stress drops produced by earthquakes. For an earthquake, the average static stress drop, $\Delta\sigma$, is given by

$$\Delta\sigma = C\mu\left(\frac{\overline{\Delta u}}{\Lambda}\right), \tag{1}$$

where $\overline{\Delta u}$ is mean slip, Λ is the characteristic rupture dimension, C is a constant that depends on rupture geometry, and μ is the shear modulus (Starr 1928; Scholz, 1990). Because the displacement–length ratio is typically 100 times greater for faults than the slip–rupture length ratio for earthquakes (Scholz, 1990), the net static stress drop is also about 100 times greater for faults. In order to calculate precisely stress drop for the volume around a rupture plane, more information is needed about the event's slip distribution than its mean slip. Because this information is often difficult to obtain, seismologists generally calculate only average static stress drop. In this study, we calculate variations in net stress drop around faults by using observed D–L profiles (Appendix A).

For an isolated fault, the elastic-plastic Dugdale model requires that the stress concentration at the fault tip must just equal the yield stress (Cowie and Scholz, 1992a). At the crack tip, material deforms plastically, while ahead of the crack tip material deforms elastically. We extend this analysis by noting that adjacent to normal faults, shear stress has fallen, except near the tips where there is a stress concentration (Fig. 6; e.g. Segall and Pollard, 1980; Willemse et al., 1996). Note that the shear stress distribution shown in Fig. 6 is for an isolated normal fault. The stress distribution around an isolated fault is a first-order approximation to the stress field around interacting faults. However, the stress distribution around two interacting faults can be quite perturbed (Segall and Pollard, 1980; Crider and Pollard, 1998). We consider only the shear stress changes induced on a locked fault by slip on a nearby fault.

For a mode III fault tip to continue to grow within the lower shear stress region (Fig. 6), the stress concentration at the crack tip must increase to balance the stress drop. This propagation criterion is expressed as

$$\sigma_{p(F)} = \sigma_y + \Delta\sigma_{(F')}, \tag{2}$$

where $\sigma_{p(F)}$ is the peak stress at the tip of fault F, σ_y is

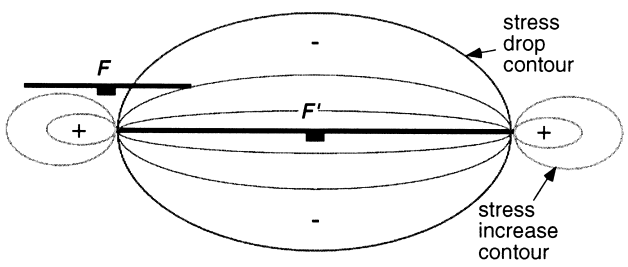

Fig. 6. Map view of the stress field around an isolated fault. Each fault is surrounded by a region of stress drop and stress increase near the tips.

the material yield strength, and $\Delta\sigma_{(F')}$ is the shear stress drop produced by a nearby fault, F', at the tip of fault F. For an isolated fault, peak stress equals yield strength, as the Dugdale model requires. For mode II tip propagation, variations in normal stress must also be considered (Segall and Pollard, 1980). One way to increase stress concentration near the tip, $\sigma_{p(F)}$, is to increase the displacement gradient.

The stress field around a fault attracts or repels other faults. Aydin and Schultz (1990) showed that underlapping fault tips are favored to propagate towards each other, while overlapping tips are retarded. If the tip of fault F is located in the region of stress increase around fault F', stress drop is negative and Eq. (2) predicts a smaller peak stress and displacement gradient (Fig. 6). If a fault F grows into a stress concentration region, it will be attracted to fault F'. Fault F may extend in length because Eq. (2) will not be balanced until its displacement gradient becomes smaller or its interacting tip reaches a region of stress drop. Faults in an underlapping configuration are rarely observed (see Aydin and Schultz, 1990), perhaps because they grow once their tips reach a high stress concentration.

In contrast, once the tip of fault F reaches the stress drop region around fault F', Eq. (2) predicts an increase in displacement near the interacting fault tip is required for the fault F to continue to propagate. In this case, one can say that fault F is repelled by fault F'. As interaction and displacement increase, stress increases in the overlap zone, which is located in the hanging wall of one fault and the footwall of the other (see Crider and Pollard, 1998). Eventually the stress may exceed the critical yield strength; at this point the overlap zone may fail and the faults may begin to coalesce.

5. Observed fault interaction

The simple model of the two-fault interaction described above can be tested by comparison with data. Displacement–length profiles for 115 faults and overlap and separation values for 65 pairs of interacting faults are archived in an electronic annex (http://veo.elsevier.nl/sg/publish/897). In a few cases, we examined interaction at each tip of a particular fault.

We analyzed faults in a pairwise fashion, as is shown in Fig. 7. Because we did not know which fault grew first, we first assumed one fault from each pair produced a stress drop region while the other fault was affected by the stress drop. As above, the fault in the role of stress drop producer is called fault F', while the fault in the role of propagator is called fault F. In order to compare the effect of fault interaction on D–L profiles for faults of different sizes, we normalized all of our data to the fault length (L') of the stress drop producer (Fig. 7). Interaction was quantified as the summed displacement anomaly in the overlapping portion of fault F, measured in standard deviations

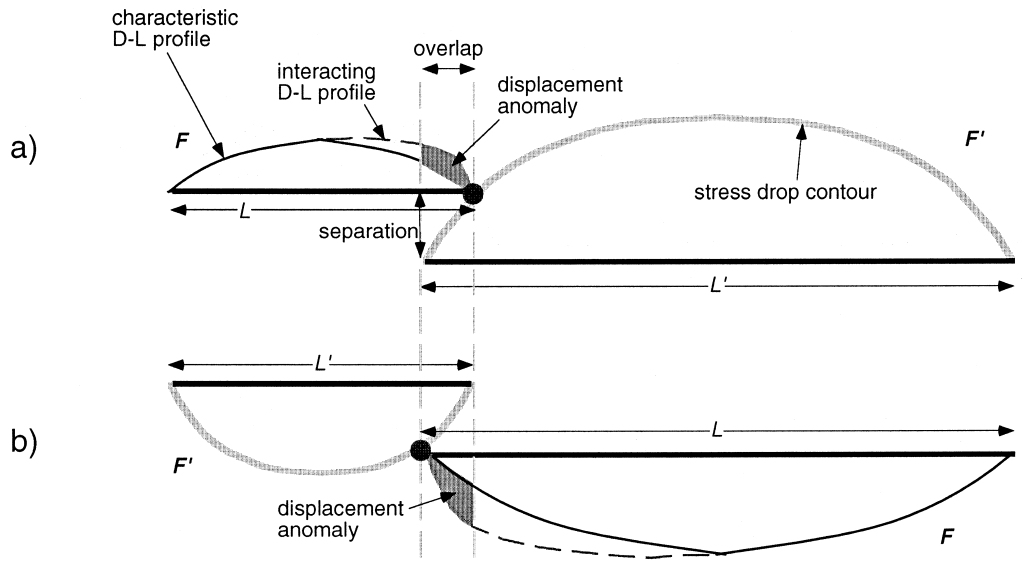

Fig. 7. Pairwise displacement anomaly analysis technique. (a) For each pair of interacting faults, one fault (F') was arbitrarily chosen, all distances were normalized to this fault's length (L') and the stress drop due to fault F' was calculated for the point where fault F ends. Displacement anomaly, measured in standard deviations from the characteristic profile, was defined to include only the anomaly within the overlapping portion of fault F. The stress drop is compared to the displacement anomaly in Figs. 8 and 9. (b) Because we did not know which fault grew first, the roles of each fault were reversed and the same analysis was repeated. Thus we obtained two stress drop and displacement anomaly measurements for each pair of faults.

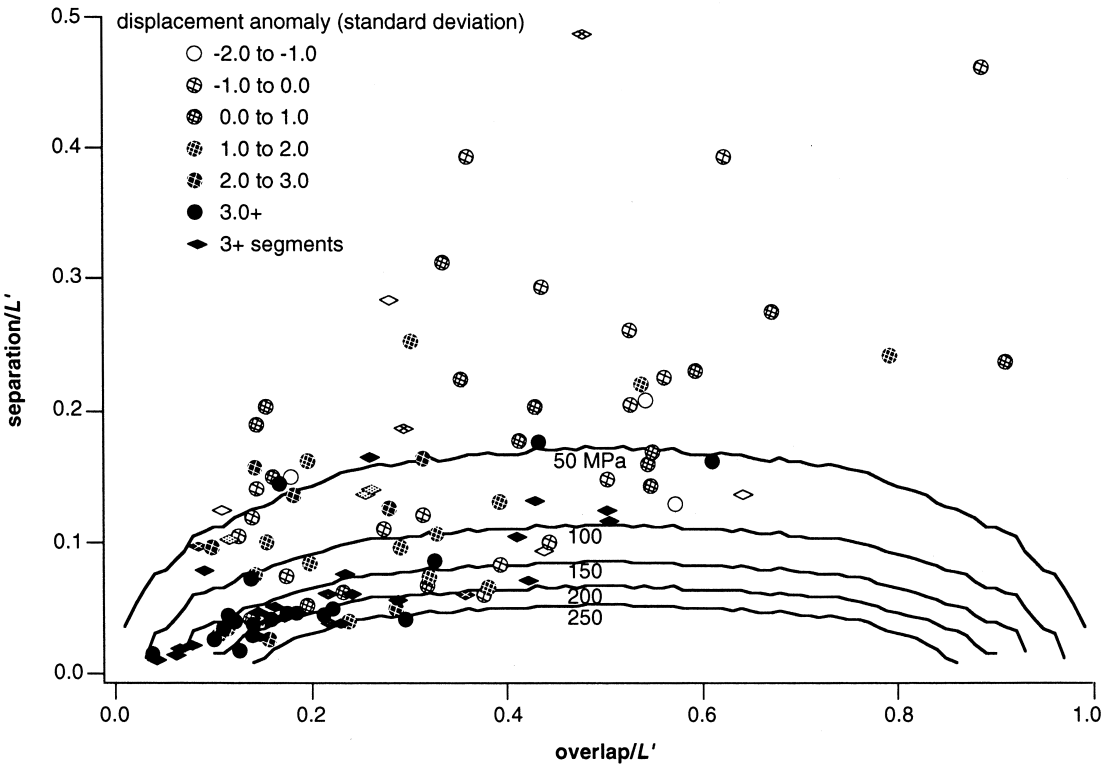

Fig. 8. Separation vs. overlap normalized to fault length as shown in Fig. 7. The shade of the symbol indicates the magnitude of the displacement anomaly in the overlapping region. Black symbols are most significant, at least three standard deviations from the characteristic profile. Lines represent stress drop contours around a fault with a characteristic profile. As described in Fig. 7, two points are plotted for each pair of interacting faults.

from the characteristic profile (Fig. 7a). Stress drop was calculated as if fault F' is isolated, has a characteristic displacement distribution (Fig. 5) and a length–width ratio of two. Information about the real displacement distribution on fault F' was not used to calculate stress drop. The method of stress drop calculation is described in Appendix A. We then switched the roles of each fault and repeated the analysis (Fig. 7b). Thus, two values of stress drop and displacement anomaly are produced for each pair of interacting faults.

Our simple model is tested by comparing these results with normalized values of overlap and separation (Fig. 8). It may be useful to visualize fault F' as initially isolated and lying along the x-axis. Curves of constant stress drop about fault F' were calculated for an isolated fault with a standard geometry using the method described in Appendix A. As the tip of fault F grows toward fault F', its growth may be affected by the stress distribution around fault F' (represented by the contours). Each symbol on Fig. 8 is placed at the point where the tip of fault F stopped growing (see Fig. 7).

Two main observations can be made with Fig. 8. First, note that faults with larger displacement anomalies (dark symbols) have grown into regions of higher stress drop. Second, none of the faults have grown into stress drop regions higher than about 200–300 MPa, as indicated by the stress drop contours.

There is a positive linear relationship between displacement anomaly on the overlapping portion of fault F and stress drop caused by fault F' (Fig. 9a). If stress drop is unrelated to displacement anomaly, we would expect 95% of the data to lie within ± 2 standard deviations of the characteristic profile, as indicated by the light dashed lines in Fig. 9(a). Only between 0 and 50 MPa is most of the data within ± 2 standard deviations of the characteristic profile. This indicates that, within the natural variation in characteristic profiles, there are no significant displacement anomalies at these low stress drops. In contrast, between 200 and 250 MPa, most displacement anomaly values are greater than $+2$ standard deviations from the characteristic profile. Thus, at high stress drop, faults have quite discernible displacement anomalies. The displacement anomaly on overlapping portions of faults clearly shows a positive dependence on stress drop, with the trend given by the solid line in Fig. 9(a). Dark dotted lines are extrapolated with the same slope as the trend line, from ± 2 standard deviations around the characteristic profile at zero stress drop. These dark dotted lines indicate that the scatter around the trend line remains approxi-

mately constant. This suggests that the scatter around the trend line is not due to interaction, but is part of the natural variation in displacement profiles.

Interacting fault pairs that are part of a multiple segment array can have higher displacement anomalies for a given stress drop than pairs that are not part of a larger array (Fig. 9b). Higher displacement anomalies in the middle of arrays are expected if these segments have greater fault plane width–length ratios (see Fig. 1b for definitions) than is assumed (Willemse, 1997). However, fault segments in the middle of arrays do not have consistently higher displacement anomalies for a given stress drop than segments on the outside of arrays.

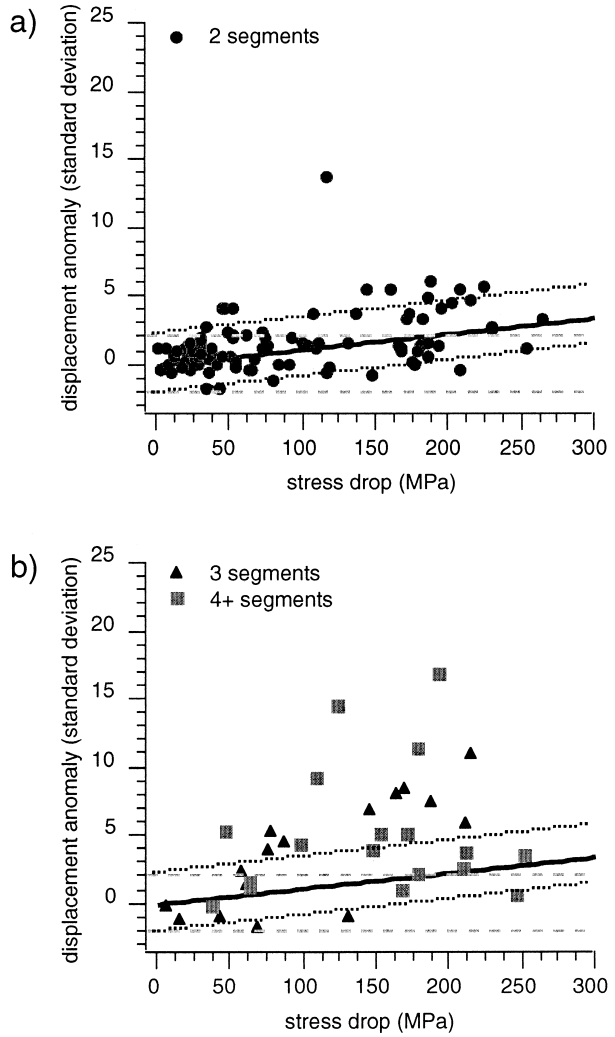

Fig. 9. Displacement anomaly of fault F vs. stress drop due to fault F'. Light dashed lines are ± 2 standard deviations around the characteristic profile; without interaction, 95% of data should lie between these lines. The solid trend line is the least squares best fit to the two-segment data and the dark dotted lines are ± 2 standard deviations extrapolated around the trend line: (a) for two interacting segments, (b) for three or more interacting segments. Lines are imposed from the two-segment data in (a).

Examples of fault pairs at different levels of interaction are shown in Fig. 10. For ease of comparison, all data are normalized to their respective fault lengths. For non-interacting faults (Fig. 10a), the profiles of individual segments are very similar to the characteristic profile; in contrast, the sum of both segments is farther from the characteristic profile. As faults grow farther into their respective stress drop fields (Fig. 10b), the individual profiles diverge from the characteristic profile, especially in overlapping portions, while the composite profile more closely resembles the characteristic profile. At some point, the combined fault profile is almost identical to a single isolated fault profile (Fig. 10c); the combined profile has a final length equal to the total length of the interacting pair. Displacement changes rapidly with distance near the tips of interacting segments, and the sum of both segments looks like the characteristic profile except for a small deficit in displacement where the two segments overlap (see also Dawers and Anders, 1995). We used the displacement anomaly along individual overlapping faults to measure interaction, but we could have quantitatively compared the summed profile to the characteristic profile as a measure of interaction.

5.1. Comparison with other observations

5.1.1. Scatter in displacement–length ratios

Although theoretical models provide the physical basis for constant D–L ratios within a population of faults (Cowie and Scholz, 1992a), this relationship has been controversial because of the large scatter observed in D–L ratios (Walsh and Watterson, 1988; Marrett and Allmendinger, 1991; Cowie and Scholz, 1992b; Gillespie et al., 1992; Dawers et al., 1993). It has been suggested by several researchers that scatter in the D–L ratio is due to fault interaction (e.g. Dawers et al., 1993; Cartwright et al., 1995; Wojtal, 1996; Willemse et al., 1996). Our results suggest that at least half of the scatter may be due to interaction. For the Solite Quarry faults, D–L ratios for the non-interacting characteristic profiles vary by a factor of 3 (Fig. 5), whereas for the whole interacting population the ratio can vary by a factor of 10 (Schlische et al., 1996).

Furthermore, the average D–L ratio of the characteristic profiles is 0.021, whereas the average for a larger data set from the Solite Quarry is 0.030 (Schlische et al., 1996). The larger population average appears to include many faults and segments that are interacting strongly with other faults. For isolated faults, D–L ratios are proportional to yield strength and inversely proportional to shear modulus (Cowie and Scholz, 1992a). For faults in an interacting population, D–L ratios also depend on the stress distributions from nearby faults (Section 4). Thus high average D–L

ratios in interacting populations can be a reflection of the level of interaction within a population as well as the material properties.

Interaction can also decrease the average D–L ratio. This will happen if, for example, two faults have linked recently and have not yet accumulated all the displacement appropriate for the size of a new single fault. However, because the average D–L ratio for the population is so much greater than for the characteristic profile, our data suggest that this effect is small. This implies that faults do not link until they have accumulated most of their composite displacement (see also Fig. 10c).

5.1.2. Separation and overlap

Separation–overlap ratios do not provide enough geometrical information about an interacting fault pair to estimate the degree of interaction between segments. Our overall separation–overlap data set is similar to those of Huggins et al. (1996) and Aydin and Schultz

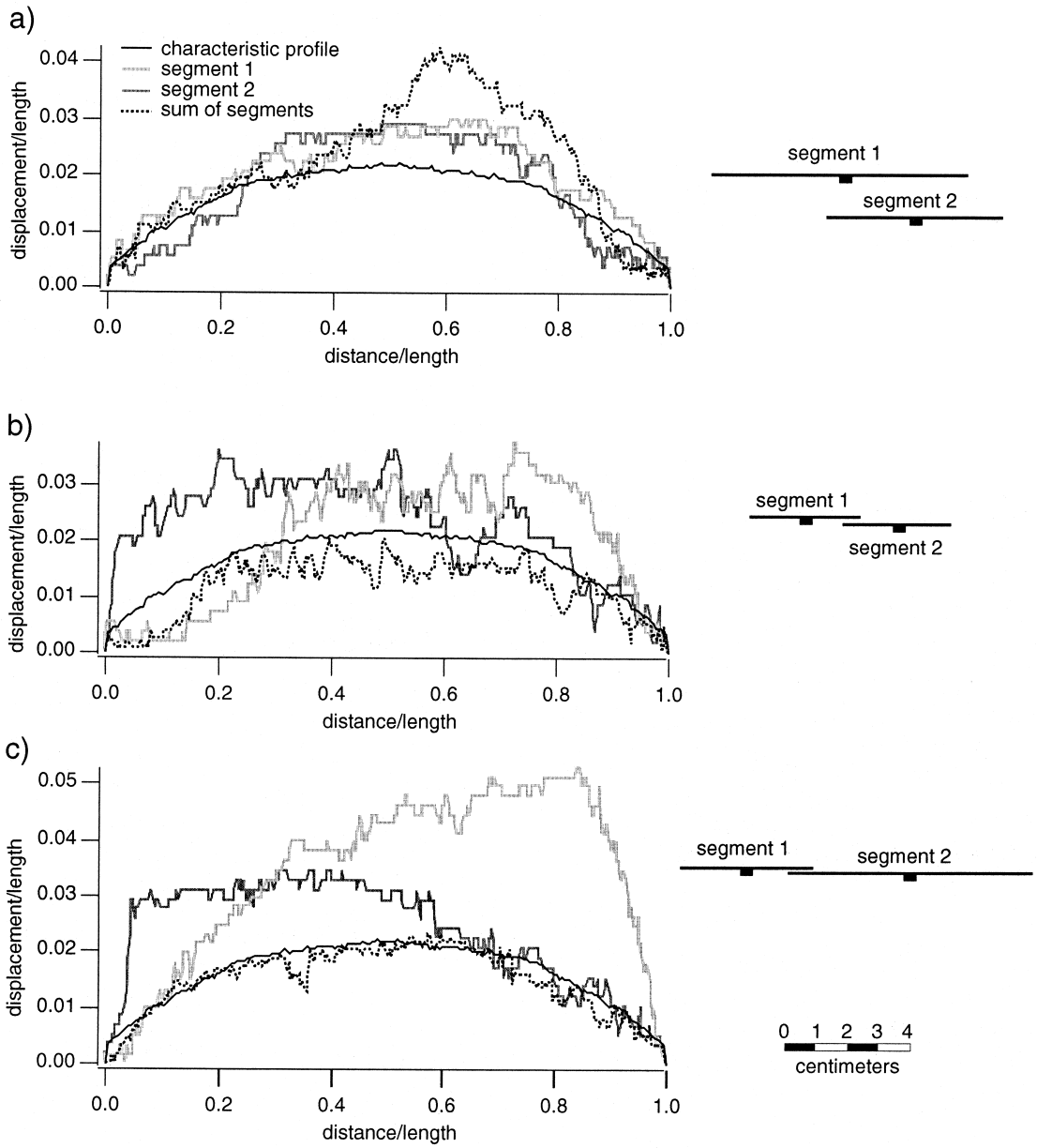

Fig. 10. Examples of fault growth with increasing interaction. All distances were normalized to length so the profiles could be directly compared to each other. The sum of both segments was normalized to the total length. The dark solid line is the characteristic profile, the shaded lines are for two separate faults, the dashed line is for their sum. The map view configuration of fault pairs are plotted to the right of profiles. (a) Fault pair which is not strongly interacting. Separation–overlap ratio is 0.33. (b) Fault pair which is interacting moderately. Separation–overlap ratio is 0.53. (c) Fault pair which is interacting very strongly and may be ready to link. Separation–overlap ratio is 0.25. Clearly, the separation to overlap ratio alone contains little information about the degree of interaction between segments.

(1990). In all data sets, separation–overlap ratios span one order of magnitude. We observe a large overall range in separation–overlap ratios (0.1–2.0), but faults with high anomalous displacement near the tips have a much narrower range, 0.1–0.35 (Fig. 11). However, faults that are not interacting strongly can also have small separation–overlap ratios (open circle in Fig. 11 and see Fig. 10). Thus, only when one first differentiates between strongly interacting and other fault pairs are separation–overlap ratios meaningful. For example, pull-apart basins have a narrow range of separation–overlap ratios (or basin dimensions) of 0.12–0.7 (Aydin and Nur, 1982). This may be because any two faults producing a pull-apart basin are physically linked already.

In contrast to separation–overlap ratios, separation and overlap values can distinguish between interacting and non-interacting fault pairs if normalized to fault length (L') and interpreted within the context of stress drop (Figs. 8 and 11). Our results show that the proximity of a fault tip (a symbol on Fig. 11) to the critical stress drop contour is a good measure of the degree of interaction between pairs of faults. In Fig. 11 we see that a separation–overlap ratio alone cannot determine the proximity of a fault tip to this critical contour. Thus overlap and separation data collected without regard to fault length is useless to determine degrees of interaction.

5.1.3. Shadow zones

Ackermann and Schlische (1997) have observed so-called shadow zones in the Solite Quarry population.

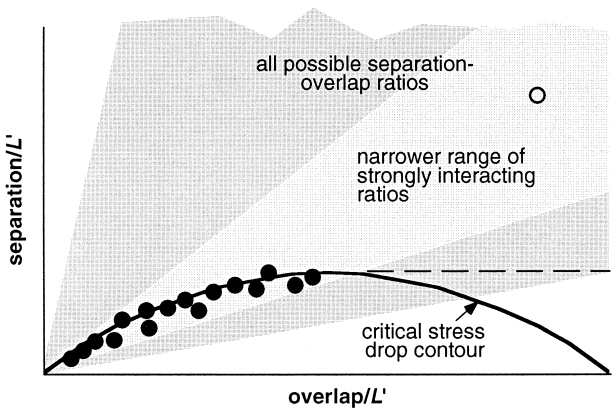

Fig. 11. Separation vs. overlap ratios. On a plot of separation vs. overlap normalized to length (L'), a constant separation–overlap ratio plots as a straight line through the origin. Solid circles represent strongly interacting pairs, open circle a non-interacting tip. By analogy with Fig. 8, we see the overall range of possible separation–overlap ratios is quite large. For strongly interacting pairs, the ratio is narrower. But even if one uses a narrow range of separation–overlap ratios to define interaction, the ratio does not distinguish between interacting faults (solid circles) and non-interacting faults (open circle).

These regions around larger faults (master faults) are devoid of other faults (Fig. 12). A linear relationship between the displacement on the master fault (d) and the perpendicular distance to the nearest fault (S) is expressed by Ackermann and Schlische (1997) as $S \approx 3d$. Faults from the Solite Quarry do not grow into stress drop regions that are higher than 200–300 MPa. The observed shadow zone boundaries occur in about the same physical location as this critical stress drop range. Using the analytical method of stress drop calculation described in Appendix A, we found $y \approx 3u(x)$ or $S \approx 3d$ for a constant stress drop of 200 MPa. The magnitude of the critical stress drop contour does not concern us here, it depends on material constants. Our point is that the critical stress drop seems to limit fault nucleation as well as fault propagation.

5.1.4. Fault interaction in the Malawi Basin, East Africa

Contreras et al. (2000) have reinterpreted seismic profiles across an array of faults in the Usisya Fault System, Malawi Basin, East Africa. There are four well-defined continuous reflectors throughout the basin, and thus one can observe these faults during three depositional intervals (Flannery and Rosendahl, 1990; Contreras et al., 2000). By assuming that the rift basin travel times are proportional to the basin depth, and that the basin depth is proportional to total displacement, relative displacement and length changes can be observed through time. In Fig. 13(a), we show an idealized map of the fault system and displacement profiles from Contreras et al. (2000). Here we omit a few very small interacting faults near the tips of the larger interacting faults. We analyzed the data for each time step in the same manner as for the faults from the Solite Quarry. We calculated displacement anomalies by comparison with the characteristic fault profile from the Solite Quarry, as the characteristic Malawi profile is unknown. Because we cannot rule out the effect of material properties, boundary conditions, and growth mechanism on the displacement profiles, only relative changes between interacting fault tips in Malawi are interpretable (Fig. 13b). We cannot determine whether the displacement anomalies are sig-

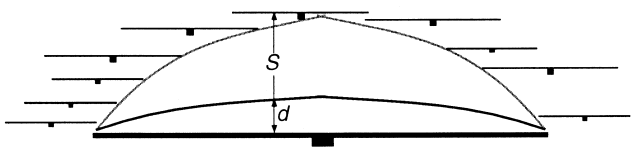

Fig. 12. 'Shadow zone' around a master normal fault and surrounding smaller faults in map view (see text for definition). Displacement, d, is shown schematically. S is the perpendicular distance from the master fault to the nearest fault (after Ackermann and Schlische, 1997).

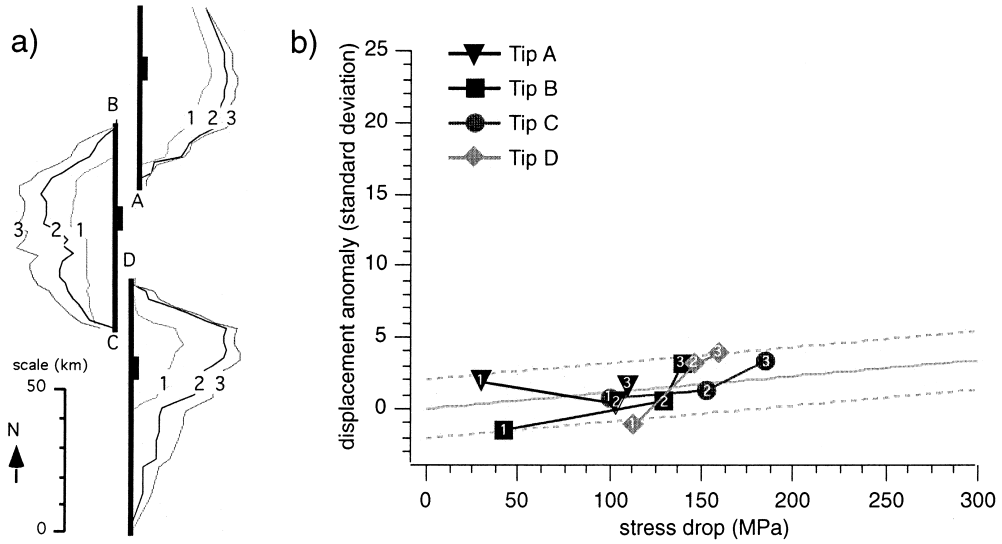

Fig. 13. (a) Idealized map view of Usisya Fault System, Malawi Rift Basin, East Africa. The profiles plotted on each fault represent the accumulation of displacement in three time steps. The final D–L ratio of the combined array is 0.03 (Contreras et al., 2000). Letters refer to fault tips and numbers to time steps. (b) Displacement anomaly vs. stress drop. The stress drop–displacement anomaly paths are plotted for the four fault tips shown in (a). Each tip has three symbols plotted, one for each time step. All fault tips start with lower stress drop and increase in stress drop in each successive time step. (Data courtesy of Contreras et al., 2000.)

nificantly different from those of isolated faults. Given these cautions, we may still gain a qualitative sense of whether displacement increases in the expected manner.

The array of faults in the Malawi basin appear to behave in a similar manner to the Solite Quarry faults. As fault tips grow into progressively higher stress drop regions, the displacement anomaly increases. However, the results suggest that this change may not occur in a completely smooth fashion. Note the interaction between tips C and D in Fig. 13(b) (circle and diamond). Both tip regions accumulate anomalous displacement as stress drop increases, but in time step 1, the region near tip C has a lower stress drop and higher displacement anomaly than the region near tip D. The situation reverses in time steps 2 and 3. This discontinuous nature suggests that large normal faults grow as expected over long time scales, but at any particular moment in time, they may exhibit a more scattered relationship between stress drop and displacement anomaly.

6. A conceptual model of fault growth

Based on our observations and simple model of fault interaction, we conclude that as a fault tip grows into any stress drop region, the displacement anomaly near the tip increases. The displacement anomaly creates a higher stress concentration near the tip, which balances the stress drop produced by the other fault. Once fault tips grow into a region of critical stress drop (200–300 MPa for the Solite Quarry population), fault tips cannot grow farther and they stop propagating or begin to link. This simple model for fault interaction is supported by our observations, which show a clear linear relationship between stress drop and displacement anomaly up to a critical value. The results provide a basis for a conceptual hypothesis for the evolution of two interacting faults into one continuous linked fault (Fig. 14). This model may be tested as we obtain more information about the ways in which faults accumulate slip. Initially, an isolated fault grows in a self-similar fashion and all parts of the fault may be actively accumulating displacement (Fig. 14a). As interaction increases, displacement anomalies increase near interacting tips, and the lateral growth of interacting tips may slow. Most displacement accumulation may occur in very specific portions of the fault plane (Fig. 14b–d). As linkage and coalescence occur, displacement accumulation may be concentrated near the center of the fault plane or in the overlap zone (Fig. 14e–f).

This displacement accumulation sequence has implications for fault growth. First, the long-term rate of growth on a particular linked fault may not be the same everywhere, rather different regions of the fault may be more active at different times with varying rates of slip. This appears to be in conflict with observations of normal faults, which show constant displacement accumulation rates over long time scales (Nicol et al., 1997). The model also suggests that the nucleation points of a particular linked fault typically are not near the maximum displacement as is often assumed.

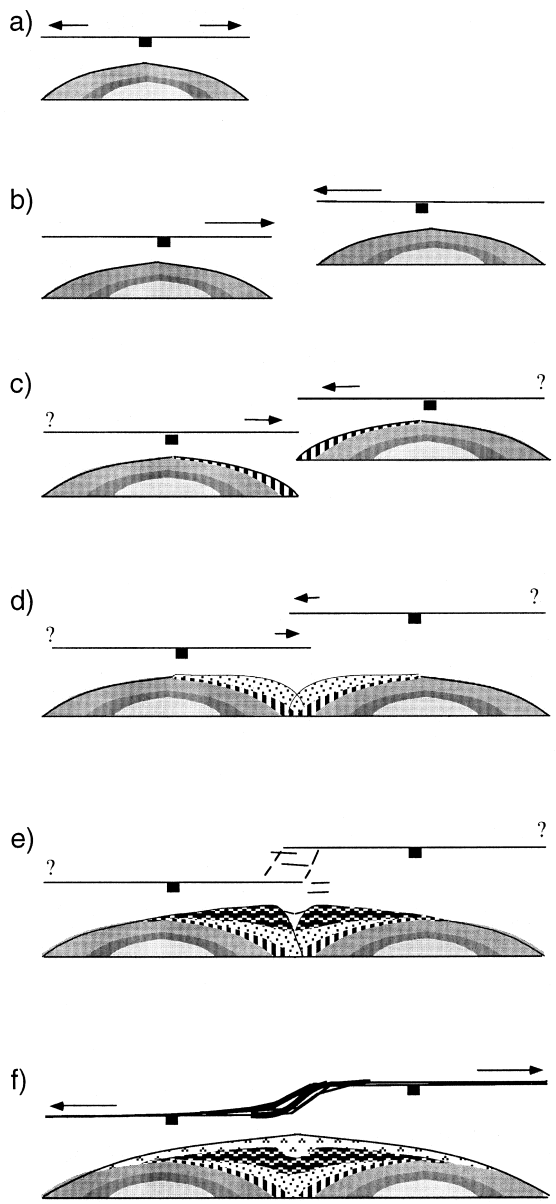

Fig. 14. Conceptual model: interaction of sub-parallel faults. (a) Pre-interaction—map view (arrows indicate propagation direction), symmetrical D–L profile is shown below. Shading represents different periods of displacement accumulation. (b) Weak interaction—while underlapping, an increase in shear stress near tips may drive faults to accelerate towards each other, until a stress drop region is reached. Underlapping faults are rarely observed. (c) Moderate interaction—after entering the stress shadow, propagation decelerates and displacement begins to accumulate near interacting tips, and steep profiles develop on interaction ends. (d) Strong interaction—any propagation is slow, displacement profiles near interacting tips steepen. Individual profiles are now very different from the characteristic profile and the composite profile is closer to the characteristic profile. (e) Linkage—once critical stress drop is reached, propagation stops, minor linkage structures form, displacement accumulates in the linkage region, and the summed profile approaches that of a single fault. (f) Coalescence—linkage is complete, the displacement profile is now appropriate for a single long fault. Propagation of distal ends resumes, leaving segment boundary behind. Portions of the overlap zone may now become part of the fault gouge.

Instead, the displacement maximum is likely to be the last place to accumulate displacement.

Knowing the degree to which fault segments interact is not only important to understanding the faults themselves, but also the structures associated with them (e.g. Segall and Pollard, 1980; Anders and Schlische, 1994; Bürgmann et al., 1994; Gawthorpe et al., 1997; Crider and Pollard, 1998; S. Gupta et al., 1998, 1999; Dawers and Underhill, 2000). As Dawers and Underhill (2000) have already observed in the case of normal faults, the basin depocenter will migrate as interaction increases. As interaction progresses, sedimentation patterns change from deposition within individual subbasins to one continuous basin (Schlische, 1993; Anders and Schlische, 1994). Throughout the early stages of fault interaction (Fig. 14b–e), sediments can be transported from the footwall, through the overlap zone, and deposited in a subbasin, although the character of the sediments may change as interaction progresses. Once coalescence occurs, the supply of footwall-derived sediments through the overlap zone may shut off (S. Gupta et al., 1999).

The continuity of summed D–L profiles across the overlap zone in advanced stages of interaction (Fig. 10c) suggests that displacement accumulation near segment boundaries depends on stress field interaction. Quantification of the degree of long-term static fault interaction (e.g. Scholz and Gupta, 2000) in conjunction with dynamic models of rupture propagation (e.g. Harris and Day, 1993) may lead to better seismic hazard estimates near interacting fault segments.

7. Summary and conclusions

We have described a model for fault interaction based on a simple elastic-plastic crack model for fault propagation and observations from the Solite Quarry normal fault population. The elastic-plastic Dugdale model assumes that the tip region is always near failure; the stress concentration at the tip must just equal the local yield strength (Cowie and Scholz, 1992a). In the case of interacting faults, the local yield strength effectively increases as shear stress drops. In order to grow in length, an interacting fault requires enough strain energy to break new fault surface ahead of the fault tip and to overcome the drop in shear stress that is produced by a nearby fault. Consequently, as a fault grows toward another fault's stress drop region, its growth is retarded. Displacement profiles and map traces from the Solite Quarry and East African Rift show that tip propagation into higher stress drop regions is proportional to displacement increase near fault tips. Anomalous displacement increases the stress concentration at an interacting tip; this provides the additional strain energy necessary for tip propagation.

Propagation into higher stress drop regions stops once a tip reaches a critical stress drop value (200–300 MPa for faults from the Solite Quarry). The physical basis for this critical value is only vaguely understood, but the observations are clear (Figs. 8 and 9). In addition, boundaries of shadow zones (Ackermann and Schlische, 1997) coincide with the critical stress drop contour, which suggests that stress drops greater than the critical value also prohibit fault nucleation.

Accumulation of anomalous displacement on interacting segments creates biases in estimates of fault population D–L ratios. Specifically, anomalous displacement accumulation leads to higher D–L ratios than would be expected for isolated faults. By comparison with our best estimate of non-interacting fault profiles, interacting faults may account for at least half the scatter in D–L ratios.

In the final stages of interaction, combined D–L profiles of interacting faults mimic that of an isolated fault (see also Dawers and Anders, 1995; Willemse et al., 1996). This observation suggests an expected sequence of displacement accumulation on interacting fault pairs. In this sequence, during advanced stages of interaction most displacement accumulates in the overlap zone. This is supported by observations of a three-segment array from the Malawi Rift Basin, East Africa. In the last stage of observed growth, displacement accumulates mostly in the middle segment (Fig. 13; Contreras et al., 2000). If correct, this sequence has consequences for sediment transport, drainage network development, and for interpretations of rift-basin stratigraphy.

We show that separation and overlap values alone do not provide enough geometrical information about an interacting fault pair to make good indicators of interaction. However, simply normalizing these values to the length of an interacting fault can provide enough information to obtain an estimate of the interaction state. By combining estimates of long-term interaction state with analysis of short-term rupture dynamics (e.g. Harris and Day, 1993), we may improve our understanding of which seismic events have high potential for rupturing interacting fault boundaries.

Acknowledgements

This research is supported by the US National Science Foundation (EAR9706475). Thoughtful reviews by D. Pollard and J. Evans helped to improve the quality of the manuscript. N. Dawers, M. Anders, M. Evans, R. Schlische and Z. Karcz provided comments on earlier versions. LDEO contribution number 6035.

Appendix A. Calculating stress drop

The simplest procedure to calculate the stress field around our isolated fault would be to use a three-dimensional (3-D) elastic crack model (e.g. Pollard and Segall, 1987). However, because the slip distribution in our standard fault is quite different from the elastic crack model in the critical region near the fault tips, this method would produce erroneous results. We used instead the following procedure.

We started with the two-dimensional solution for deflection of a horizontal surface, w, due to a vertical screw dislocation with constant offset (e.g. Contreras et al., 1997) and modified it to incorporate changes in slip and depth:

$$w(x,y) = \frac{-u(x)}{\pi}\left(\arctan\left(\frac{H}{y}\right)\right). \tag{A-1}$$

The x-axis runs along fault strike, the y-axis is perpendicular to the fault plane, $u(x)$ is the characteristic slip distribution for a particular population (Fig. 5), and H is the dislocation depth, which we discuss below. All distances were normalized to fault length. However, the true slip distribution is 3-D (Fig. A1a); we must approximate a 3-D geometry with an analytical, two-dimensional solution.

The depth of the dislocation, H, will be

$$H = C_2 L \tag{A-2}$$

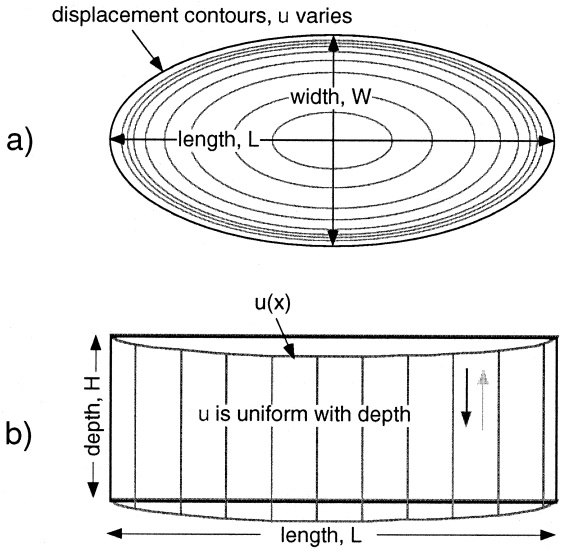

Fig. A1. (a) A realistic fault plane from Solite Quarry has an elliptical tip line and displacement varies from D_{max} near the center to zero at the tip line. (b) Dislocation geometry: We use a rectangular dislocation and uniform displacement with depth, equal to the surface displacement, $u(x)$, to approximate the displacement field. We must scale H properly to obtain a reasonable approximation to the actual displacement field.

where C_2 is a constant that depends on the slip distribution and shape of the fault plane. The depth of Solite Quarry faults, $h(x)$, typically varies from zero near the mode III tips to $L/4$ near the center of the fault plane (Fig. A2). We approximate the variable fault plane depth, $h(x)$, with $H = h_{avg} \approx L/8$. We also assume the slip is uniform with depth as is equal to the surface slip, $u(x)$ (Fig. A1b). Because slip must actually decrease towards zero at the base of the fault (Fig. A1a), our approximation of uniform slip with depth will produce too broad a surface displacement field. This can be approximately compensated for by assuming a fault of half the actual depth, i.e. $H \approx L/16$. See Mavko (1981) for the equivalent demonstration for a strike-slip fault. Hence $C_2 = 1/16$.

We obtained a displacement field due to a rectangular screw dislocation using Eq. (A-1) with the measured slip distribution, $u(x)$, and C_2 as above. We compared this displacement field to the numerical solution for the displacement field around an isolated fault obtained by Gupta and Scholz (1998). This was a 3-D boundary element model with an elastic rheology and input of known displacement distribution on an isolated fault plane (e.g. Fig. A1a). We found the average least-squares best fit of the displacement field described by Eq. (A-1) to the boundary element model occurred when $H = 0.059$. The dislocation solutions given by the two different values of H (0.059 and 0.063) are almost indistinguishable.

We then took the partial derivative of deflection, w, with respect to y to obtain shear strain:

$$\varepsilon_{zy} = \frac{1}{2}\left(\frac{\partial w}{\partial y} + \frac{\partial v}{\partial z}\right) = \frac{u(x)H}{2\pi y^2}\left(1 + \left(\frac{H}{y}\right)^2\right)^{-1}. \qquad \text{(A-3)}$$

We neglected the contribution to shear strain from $\partial v/\partial z$, the change in displacement in the y-direction with depth, because it is small relative to the change in deflection, w. Once strain was calculated using Eq. (A-3), we multiplied strain by the shear modulus, μ, to obtain the shear stress drop distribution around a fault with a characteristic displacement distribution:

$$\Delta\sigma = \mu\varepsilon_{zy}. \qquad \text{(A-4)}$$

In Section 5, we used this analytical method to calculate stress drop around isolated faults.

We assumed a shear modulus typical of shale or sandstone, 1×10^{10} Pa (Turcotte and Schubert, 1982).

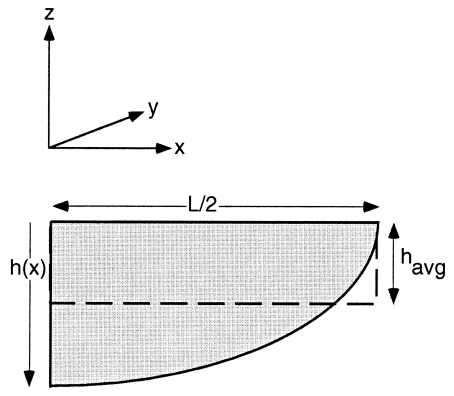

Fig. A2. A quarter of the fault plane used to illustrate scaling of H.

References

Ackermann, R.V., Schlische, R.W., 1997. Anticlustering of small normal faults around larger faults. Geology 25, 1127–1130.

Amato, A., Azzara, R., Chiarabba, C., Cimini, G.B., Cocco, M., Di Bona, M., Margheriti, L., Mazza, S., Mele, F., Selvaggi, G., Basili, A., Boschi, E., Courboulex, F., Deschamps, A., Gaffet, S., Bittarelli, G., Chiaraluce, L., Piccinini, D., Ripepe, M., 1998. The 1997 Umbria–Marche, Italy, earthquake sequence: a first look at the main shocks and aftershocks. Geophysical Research Letters 25, 2861–2864.

An, L.J., 1997. Maximum link distance between strike-slip faults: observations and constraints. Pure and Applied Geophysics 150, 19–36.

Anders, M.H., Schlische, R.W., 1994. Overlapping faults, intrabasin highs, and the growth of normal faults. Journal of Geology 102, 165–180.

Aydin, A., Nur, A., 1982. Evolution of pull-apart basins and their scale independence. Tectonics 1, 91–105.

Aydin, A., Schultz, R.A., 1990. Effect of mechanical interaction on the development of strike-slip faults with échelon patterns. Journal of Structural Geology 12, 123–129.

Barnett, J.A.M., Mortimer, J., Rippon, J.H., Walsh, J.J., Watterson, J., 1987. Displacement geometry in the volume containing a single normal fault. American Association of Petroleum Geologists Bulletin 71, 925–937.

Bürgmann, R., Pollard, D.D., Martel, S.J., 1994. Slip distributions on faults: Effects of stress gradients, inelastic deformation, heterogeneous host-rock stiffness, and fault interaction. Journal of Structural Geology 16, 1675–1690.

Cartwright, J.A., Mansfield, C.S., 1998. Lateral displacement variation and lateral tip geometry of normal faults in the Canyonlands National Park, Utah. Journal of Structural Geology 20, 3–19.

Cartwright, J.A., Trudgill, B.D., Mansfield, C.S., 1995. Fault growth by segment linkage: an explanation for scatter in maximum displacement and trace length data from the Canyonlands Grabens of SE Utah. Journal of Structural Geology 17, 1319–1326.

Childs, D., Watterson, J., Walsh, J.J., 1995. Fault overlap zones within developing normal fault systems. Journal of the Geological Society of London 152, 535–549.

Cladouhos, T.T., Marrett, R., 1996. Are fault growth models consistent with power-law distributions of fault lengths? Journal of Structural Geology 18, 281–293.

Contreras, J., Scholz, C.H., King, G.C.P., 1997. A model of rift basin evolution constrained by first-order stratigraphic observations. Journal of Geophysical Research 102, 7673–7690.

Contreras, J., Anders, M.H., Scholz, C.H., 2000. Kinematics of normal fault growth and fault interaction in the Central Part of Lake Malawi Rift. Journal of Structural Geology 22, 159–168.

Cowie, P.A., 1998. A healing–reloading feedback control on the growth rate of seismogenic faults. Journal of Structural Geology 20, 1075–1087.

Cowie, P.A., Scholz, C.H., 1992a. Physical explanation for the dis-

placement–length relationship of faults using a post-yield fracture mechanics model. Journal of Structural Geology 14, 1133–1148.

Cowie, P.A., Scholz, C.H., 1992b. Displacement–length scaling relationship for faults: Data synthesis and discussion. Journal of Structural Geology 14, 1149–1156.

Crider, J.G., Pollard, D.D., 1998. Fault linkage: three-dimensional mechanical interaction between echelon normal faults. Journal of Geophysical Research 103, 24373–24391.

Dawers, N.H., Anders, M.H., 1995. Displacement–length scaling and fault linkage. Journal of Structural Geology 17, 604–614.

Dawers, N.H., Anders, M.H., Scholz, C.H., 1993. Growth of normal faults: Displacement–length scaling. Geology 21, 1107–1110.

Dawers, N.H., Underhill, J.R., 2000. The role of fault interaction and linkage in controlling syn-rift stratigraphic sequences: Statfjord East area, Northern North Sea. American Association of Petroleum Geologists Bulletin 84, 45–64.

Flannery, J.W., Rosendahl, B.R., 1990. The seismic stratigraphy of Lake Malawi, Africa: Implications for interpreting geological processes in lacustrine rifts. Journal of African Earth Science 10, 519–548.

Gawthorpe, R.L., Sharp, I., Underhill, J.R., Gupta, S., 1997. Linked sequence stratigraphic and structural evolution of propagating normal faults. Geology 25, 795–798.

Gillespie, P.A., Walsh, J.J., Watterson, J., 1992. Limitations of dimension and displacement data from single faults and the consequences for data-analysis and interpretation. Journal of Structural Geology 14, 1157–1172.

Gupta, A., Scholz, C.H., 1998. Utility of elastic models in predicting fault displacement fields. Journal of Geophysical Research 103, 823–834.

Gupta, S., Underhill, J.R., Sharp, I.R., Gawthorpe, R.L., 1999. Role of fault interactions in controlling synrift sediment dispersal patterns: Miocene, Abu Alaqa Group, Suez Rift, Sinai, Egypt. Basin Research 11, 167–189.

Gupta, S., Cowie, P.A., Dawers, N.H., Underhill, J.R., 1998. A mechanism to explain rift-basin subsidence and stratigraphic patterns through fault-array evolution. Geology 26, 595–598.

Harris, R.A., Day, S.M., 1993. Dynamics of fault interaction: parallel strike-slip faults. Journal of Geophysical Research 98, 4461–4472.

Huggins, P., Watterson, J., Walsh, J.J., Childs, C., 1996. Relay zone geometry and displacement transfer between normal faults recorded in coal-mine plans. Journal of Structural Geology 17, 1741–1755.

Jones, L., Aki, K., Boore, D., Celebi, M., Donnellan, A., Hall, J., Harris, R., Hauksson, E., Heaton, T., Hough, S., Hudnut, K., Hutton, K., Johnston, M., Joyner, W., Kanamori, H., Marshall, G., Michael, A.J., Murray, M., Ponti, D., Reasenberg, P., Schwartz, D., Seeber, L., Shakal, A., Simpson, R., Mori, J., Thio, H., Tinsley, J., Todorovska, M., Trifunac, M., Wald, D., Zoback, M.L., 1994. The magnitude—6.7 Northridge, California Earthquake of 17-January-1994. Science 266, 389–397.

Marrett, R., Allmendinger, R.W., 1991. Estimates of strain due to brittle faulting—sampling of fault populations. Journal of Structural Geology 13, 735–738.

Mavko, G.M., 1981. Mechanics of motion on major faults. Annual Review of Earth and Planetary Sciences 9, 81–111.

Muraoka, H., Kamata, H., 1983. Displacement distribution along minor fault traces. Journal of Structural Geology 5, 483–495.

Nicol, A., Walsh, J.J., Watterson, J., Underhill, J.R., 1997. Displacement rates of normal faults. Nature 390, 157–159.

Peacock, D.C.P., Sanderson, D.J., 1991. Displacements, segment linkage and relay ramps in normal fault zones. Journal of Structural Geology 13, 721–733.

Peacock, D.C.P., Sanderson, D.J., 1994. Geometry and development of relay ramps in normal fault systems. American Association of Petroleum Geologists Bulletin 78, 147–165.

Pollard, D.D., Segall, P., 1987. Theoretical displacements and stresses near fractures in rock: with applications to faults, joints, veins, dikes, and solution surfaces. In: Atkinson, B.K. (Ed.), Fracture Mechanics of Rock. Academic Press, London, pp. 277–349.

Rippon, J.H., 1985. Contoured patterns of throw and hade of normal faults in the Coal Measures (Westphalian) of northwest Derbyshire. Proceedings of the Yorkshire Geological Society 45, 147–161.

Schlische, R.W., 1993. Anatomy and evolution of the Triassic–Jurassic continental rift system, Eastern North America. Tectonics 12, 1026–1042.

Schlische, R.W., Young, S.S., Ackermann, R.V., Gupta, A., 1996. Geometry and scaling relations of a population of very small rift-related normal faults. Geology 24, 683–686.

Scholz, C.H., 1990. The Mechanics of Earthquakes and Faulting. Cambridge University Press, Cambridge, UK.

Scholz, C.H., Gupta, A., 2000. Fault interactions and seismic hazard. Journal of Geodynamics 29, 459–467.

Segall, P., Pollard, D.D., 1980. Mechanics of discontinuous faults. Journal of Geophysical Research 85, 4337–4350.

Sieh, K., Jones, L., Hauksson, E., Hudnut, K., Eberhart-Phillips, D., Heaton, T., Hough, S., Hutton, K., Kanamori, H., Lilje, A., Lindvall, S., McGill, S.F., Mori, J., Rubin, C., Spotila, J.A., Stock, J., Thio, H.K., Treiman, J., Wernicke, B., Zachariasen, J., 1993. Near-field investigations of the Landers earthquake sequence, April to July 1992. Science 260, 171–176.

Starr, A., 1928. Slip in a crystal and rupture in a solid due to shear. Proceedings of the Cambridge Philosophical Society 24, 489–500.

Turcotte, D.L., Schubert, G., 1982. Geodynamics: Applications of Continuum Physics to Geological Problems. John Wiley & Sons, New York.

Walsh, J.J., Watterson, J., 1988. Analysis of the relationship between displacements and dimensions of faults. Journal of Structural Geology 10, 239–247.

Wesnousky, S.G., 1986. Earthquakes, Quaternary faults, and seismic hazard in California. Journal of Geophysical Research 91, 12587–12631.

Willemse, E.J.M., 1997. Segmented normal faults: correspondence between three dimensional mechanical models and field data. Journal of Geophysical Research 102, 675–692.

Willemse, E.J.M., Pollard, D.D., Aydin, A., 1996. Three-dimensional analyses of slip distributions on normal fault arrays with consequences for fault scaling. Journal of Structural Geology 18, 295–309.

Wojtal, S.F., 1996. Changes in fault displacement populations correlated to linkage between faults. Journal of Structural Geology 18, 265–279.